International Journal of Power Electronics and Drive System (IJPEDS)
Vol. 17, No. 4, December 2026, pp. 2669~2680
ISSN: 2088-8694, DOI: 10.11591/ijpeds.v17.i4.pp2669-2680

Reducing complexity for predictive current control for PMSM created on a developed target function

Yasameen H. Abdulrida[1], Islam Khalid[2], Othman J. Alhayali[3]
[1]Ibn Sina University of Medical and Pharmaceutical Sciences, Baghdad, Iraq
[2]Department of Power and Electrical Machines Engineering, College of Engineering, Diyala University, Diyala, Iraq
[3]Renewable Energy Research Center, University of Anbar, Anbar, Iraq

Article Info

Article history:

Received Mar 5, 2026
Revised Aug 24, 2026
Accepted Oct 4, 2026

Keywords:

Delay compensation
Factor robustness
Flux-weakening control
Model predictive control
Objective function

ABSTRACT

When requesting a definite control set model predictive control (FCS-MPC) for mobility weakening control of permanent-magnet synchronous machines (PMSM), issues arose related to the limit-strength standard. To address these issues, we propose a proportional-integral-derivative (PID)-type cost function specifically designed for FCS-MPC in this framework. This cost function comprises three parts: an equivalent error cost that focuses on current following, a basic error cost to reduce steady-state control errors, and a characteristic wrong cost proposed to reduce ripple errors. In this group, the cost function is used to implement delay compensation to improve prediction accuracy in the control system. Simulation results show that when the PMSM limits are misaligned and with on-diluting control, the FCS-MPC establishes a type cost function that forces the control system's robustness to engine limits and load-force disturbances, while maintaining attractive dynamic characteristics. Notably, this control strategy reduces the total harmonic distortion (THD) of the three-phase current from 13.09% to 4.79% and reduces the ripple force by 50% to 5.75%.

This is an open access article under the CC BY-SA license.

Corresponding Author:

Yasameen H. Abdulrida
Ibn Sina University of Medical and Pharmaceutical Sciences
Baghdad, Iraq
Email: yasameen.aarajy@ibnsina.edu.iq

1. INTRODUCTION

Permanent magnet synchronous motors (PMSMs) offer simple construction, great efficiency, and a wide speed regulation range, and are generally utilized in electric vehicles [1], [2]. To improve PMSM control performance, researchers have developed many advanced control algorithms. In recent years, finite-set model predictive control (MPC) has received increasing attention [3], [4]. Finite control set model predictive control (FCS-MPC) offers a simple control structure, an intuitive control principle, and an objective function that enables multi-objective collaborative control [5], [6]. Predicting the control quantity is a prerequisite for FCS-MPC control. The cost function has decisive significance for the control objective. Therefore, different optimization objectives can be achieved by improving the cost function [7]. However, FCS-MPC control performance depends heavily on model parameters and suffers from poor parameter robustness. At present, domestic and foreign scholars mainly focus on multi-objective collaboration [8], [9], and little research has addressed system-parameter robustness.

On the other hand, to meet the requirements of an extensive speed regulation range of the PMSM system for electric vehicles, the control strategy usually adopts maximum torque per ampere (MTPA) control below the base speed; above the base speed, the motor speed is further increased by weak magnetic control [10], [11]. In this process, especially in the high-speed, weakly magnetic region, PMSM inductance varies with the degree of magnetic circuit saturation, and resistance and permanent-magnet flux vary with

temperature. These changes in motor parameters will increase the FCS-MPC current-control error, affecting the scheme's performance [12]. To improve the robustness of FCS-MPC parameters in PMSM control, a prediction-error compensation strategy is proposed. When PMSM parameters are mismatched, online error compensation improves the accuracy of the model-predicted current [13], [14]. However, this strategy requires updating the prediction-error information, which can lead to a stagnant state and inaccurate current prediction. This addresses the problem that FCS-MPC is highly dependent on the prediction model, and that model mismatch can lead to larger prediction errors [15]. This paper proposes a prediction-error compensation scheme based on the expanded state observer (ESO). This method employs a two-step prediction process and uses ESO observation results to build a prediction model for delay compensation. Still, it increases the computational complexity of the prediction link. It introduces a method for online identification of motor inductance factors. By adjusting motor inductance in real time, the model parameters improve, thereby achieving better control performance [16]. However, in addition to inductance, the motor parameters include resistance, permanent magnet flux, and other factors. Identifying all parameters simultaneously will cause a rank problem. Therefore, parameter identification methods generally identify only a few key parameters, and their accuracy is affected by factors such as saturation and inverter dead zone, making it difficult to achieve high accuracy in practice.

In [17], a dual-vector duty cycle method was introduced by tracking the stator flux-linkage error and constructing a value function. The duration of the selected voltage vector was calculated utilizing the deadbeat idea concept and the principle of minimizing the value function. This method cannot reduce the flux-linkage error over the cycle. In [18], the duty cycle algorithm was further improved. Based on the deadbeat idea, the time required for the q-axis current to track the reference value was calculated, and the optimal effective vector was selected. This reduced electromagnetic torque fluctuations and improved system performance. In [19], the authors proposed an improved dual-vector MPCC algorithm. This method combines the zero vector and the effective voltage vector in each sector to form a desired voltage vector. It then selects the voltage vector with the smallest cost function value as the ideal voltage vector.

Finally, the authors implemented deadbeat control of the d-q-axis current and determined the deadbeat-calculated voltage-vector action period. In [20], the problem of voltage-vector combination sequence was solved by q-axis deadbeat control, but the number of switching combinations was large. To a considerable extent, it affected the control performance. Although researchers have adopted a dual-vector MPC method based on the deadbeat concept to achieve optimal output in a single control cycle, they have neglected the current error generated within the cycle and thus have not achieved global optimality. In [21], field-weakening speed-extension methods based on FCS-MPC were proposed. However, the aforementioned papers did not address research on square-wave operation methods. To achieve square-wave operation of FCS-MPC, the objective function of traditional FCS-MPC can be modified by adding a weight to the switching frequency and using a larger weighting factor. Although this can achieve near-square-wave control in the field-weakening domain, it degrades motor control performance in the linear speed range, making it difficult to find the optimal balance point for the weighting factor.

Although FCS-MPC-based PMSM drives have made significant progress, challenges remain under mismatched parameters and during field weakening at high speeds. Existing techniques use observers, parameter estimation, robust prediction, duty cycle optimization, or modified modulation structures, which increase control complexity. To overcome these limitations, this study proposes incorporating a cost function directly into the traditional FCS-MPC framework, similar to a proportional-integral-derivative (PID)-type cost function. The proposed approach combines the finite-control-set and direct-switching properties of FCS-MPC with an integral- and prediction-based difference-error term to minimize persistent current-tracking errors and reduce current ripple. Thus, the primary novelty of the FCS-MPC cost function is not to change the predictive-control structure but to improve its robustness under field-weakening operation.

To address the parameter-sensitivity drawback of the PMSM system created with FCS-MPC, this paper proposes applying FCS-MPC with a PID-type cost function (PID-MPC for short) for PMSM magnetic-field weakening control. When the prediction-model parameters in the low-speed MTPA area and the high-speed magnetic-field-weakening area are mismatched, PID-MPC uses integral and differential error terms in the objective function to calculate the optimal factors. The differential term suppresses steady-state current error and current ripple, improving the robustness of the FCS-MPC parameter set while preserving the excellent dynamic performance of traditional FCS-MPC.

2. METHOD

2.1. Mathematical model of PMSM

To establish the numerical model of the d- and q-axes of a PMSM, we first assume that: 1) The saturation of the core is ignored; 2) Eddy current and hysteresis losses are ignored; and 3) The stator current

is a symmetrical 3-phase sinusoidal current. Thus, the numerical model of the PMSM in the d-q coordinate system is obtained [22], [23]. The voltage is (1).

$$\begin{cases} u_d = L_d \frac{\mathrm{d}i_d}{\mathrm{d}t} + R_\mathrm{s} i_d - \omega_\mathrm{e} L_q i_q \\ u_q = L_q \frac{\mathrm{d}i_q}{\mathrm{d}t} + R_\mathrm{s} i_q + \omega_\mathrm{e} L_d i_d + \omega_\mathrm{e} \psi_\mathrm{f} \end{cases} \quad (1)$$

The torque equation is (2).

$$T_\mathrm{e} = \frac{3}{2} p_\mathrm{n} \left[\psi_\mathrm{f} i_q + \left(L_d - L_q \right) i_d i_q \right] \quad (2)$$

Where: u_d、u_q Are the d- and q-axis voltages, respectively, and i_d、i_q are the d-and q-axis currents, respectively. and L_d、L_q are the d-and q-axis inductances, respectively. R_s is the stator resistance; ω_e is the rotor's electrical angular velocity; ψ_f Is the rotor permanent magnet flux, and p_n Is the number of motor pole pairs.

2.2. 3-phase voltage source inverter

The three-phase voltage source inverter (VSI) is a basic power electronic device that converts a DC-link voltage into a balanced three-phase AC voltage. It is commonly employed in motor drives, renewable energy conversion systems, and power conditioning applications [24]. This is a three-phase VSI with three legs (phases), an upper controlled switch (usually an IGBT or MOSFET) with antiparallel diodes, and a lower controlled switch with antiparallel diodes. The midpoints of each of the four legs are joined to the load legs a, b, and c [25]. The topology of the 3-phase-2-level (3-P2-L) VSI is illustrated in Figure 1. The voltage across the DC-link is called V_{dc}. The switching states of the upper and lower switches in each leg are represented by S_x and $\bar{S}_x (\mathrm{x} = \mathrm{a}, \mathrm{b}, \mathrm{c})$, respectively, where: $S_x = 1$: upper switch is ON, $\bar{S}_x = 1$: lower switch is ON, $S_x + \bar{S}_x = 1$: complementary switching. The output voltages of the phases, with respect to the negative DC bus (N), are:

$$v_{xN} = \begin{cases} \frac{V_{dc}}{2}, & \text{if } S_x = 1 \\ -\frac{V_{dc}}{2}, & \text{if } S_x = 0 \end{cases} \quad x = a, b, c \quad (3)$$

These voltages can be written compactly as $v_{xN} = (2S_x - 1)\frac{V_{dc}}{2}$.

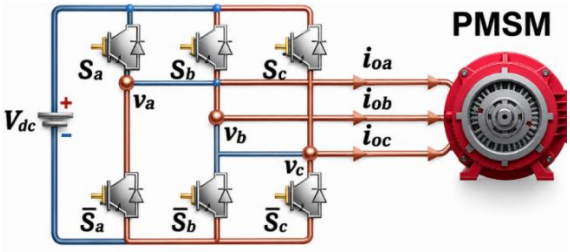

Figure 1. 3-phase, 2-level VSI and PMSM drive topology

2.3. Principle of field weakening control

The concept of PMSM field-weakening control is to utilize the armature reaction of the air-gap magnetic field. By adjusting the stator current distribution, the main magnetic field is weakened, thereby increasing the motor's d-axis demagnetizing current element and dropping the q-axis current element to maintain voltage balance during high-speed operation [26]. This is known as field weakening control. Due to the limitations of the inverter's maximum voltage output capability and maximum allowable current, the current and voltage constraint equations for the PMSM in the d-q coordinate system are:

$$i_d^2 + i_q^2 = i_\mathrm{s}^2 \leqslant I_\mathrm{max}^2 \quad (4)$$

$$u_d^2 + u_q^2 = u_\mathrm{s}^2 \leqslant U_\mathrm{max}^2 \quad (5)$$

where i_s and u_s are the motor stator current and voltage, respectively. When the PMSM is operating at great speed, the motor's resistance is much smaller than its reactance, so the voltage drops across the resistor can be ignored. The steady-state voltage equation at high speed is (6).

$$\begin{cases} u_d = -\omega_e L_q i_q \\ u_q = \omega_e L_d i_q + \omega_e \psi_f \end{cases} \quad (6)$$

Replacing equivalence (5) with equivalence (4), the voltage equivalence is (7).

$$\left(L_q i_q\right)^2 + (L_d i_d + \psi_f)^2 \leqslant \left(\frac{U_{max}}{\omega_e}\right)^2 \quad (7)$$

Figure 2 displays the allowable operating region of the PMSM in the id−iq plane under the current and voltage limits. The current-limit circle is the max acceptable magnitude of the stator current, and the voltage-limit ellipses are the available voltage capability at various operating speeds. The max torque per current trajectory and the max torque per voltage trajectory define the max-current operating points for high-torque capability, given the constraints. As the speed increases (from ω1 to a higher operating condition), the feasible region becomes smaller due to voltage limitations, and the d- and q-axis currents need to be adjusted accordingly. The marked operating points indicate the transition between the torque-producing and field-weakening regions, highlighting the need for coordinated current control to ensure optimal PMSM performance at high speeds.

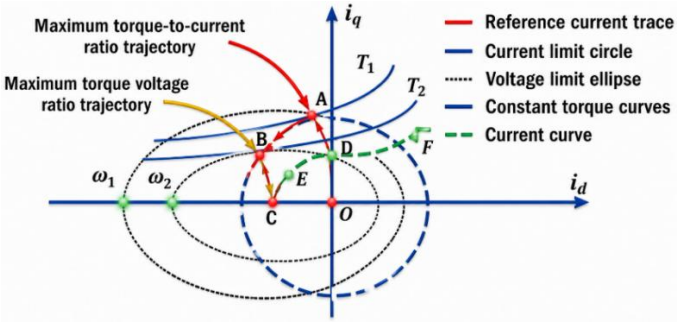

Figure 2. Reference current trajectory for field weakening in a PMSM

3. FCS-MPC CURRENT CONTROL OF PMSM

3.1. Prediction model

The prediction model for the PMSM after discretizing (1) using the Euler method is:

$$\begin{cases} i_{d(k+1)}^p = \frac{T_s}{L_d} u_{d(k)} + \left(1 - \frac{T_s R_s}{L_d}\right) i_{d(k)} + T_s \omega_e i_{q(k)} \\ i_{q(k+1)}^p = \frac{T_s}{L_q} u_{q(k)} + \left(1 - \frac{T_s R_s}{L_q}\right) i_{q(k)} + T_s \omega_e i_{d(k)} - \frac{T_s \omega_e \psi_f}{L_q} \end{cases} \quad (8)$$

where: is the sampling period; the superscript p is the predicted value; and are the current values on the d and q axes at period k; and are the voltage values on the d and q axes at period k [27]. The Park transform can obtain this.

$$\begin{cases} u_d = u_\alpha \cos\theta + u_\beta \sin\theta \\ u_q = -u_\alpha \sin\theta + u_\beta \cos\theta \end{cases} \quad (9)$$

Where θ is the electrical angle of the rotor. The voltages in the α, β-organized scheme can be obtained from the inverter switching state in Table 1. When the microcontroller works, there is a 2-cycle delay between the control algorithm and the sampling period [28]. Considering the adverse effect of system delay on motor performance, a delay-compensation approach is adopted for the system, as predicted by (7). The current at time k+2 is:

$$\begin{cases} i_{d(k+2)}^{p} = \frac{T_s}{L_d} u_{d(k+1)} + \left(1 - \frac{T_s R_s}{L_d}\right) i_{d(k+1)} + T_s \omega_e i_{q(k+1)} \\ i_{q(k+2)}^{p} = \frac{T_s}{L_q} u_{q(k+1)} + \left(1 - \frac{T_s R_s}{L_q}\right) i_{q(k+1)} + T_s \omega_e i_{d(k+1)} - \frac{T_s \omega_e \psi_f}{L_q} \end{cases} \quad (10)$$

Table 1. Switching table of the inverter

$S_{abc} = (S_a S_b S_c)$	000	001	010	011	100	101	110	111
u_α	0	$-U_{DC}/3$	$-U_{DC}/3$	$-U_{DC} \times 2/3$	$U_{DC} \times 2/3$	$U_{DC}/3$	$U_{DC}/3$	0
u_β	0	$-U_{DC}/\sqrt{3}$	$U_{DC}/\sqrt{3}$	0	0	$-U_{DC}/\sqrt{3}$	$U_{DC}/\sqrt{3}$	0

3.2. Traditional objective function

According to (8), the current values of the inverter's eight switching states are predicted and substituted into (10) for evaluation. The FCS-MPC with the traditional objective function selects the switching state that yields the lowest objective function value as the ideal solution and outputs it in the next cycle. From the above analysis, the traditional cost function aims to minimize the control error between the predicted current and the reference current. Still, it does not consider the accuracy of the motor prediction model [29]. During motor operation, the motor's inductance varies with the degree of magnetic-circuit saturation, and the resistance and permanent-magnet flux vary with temperature. In the weakly magnetic, high-speed region, inductance coupling deepens. Uncertainty in these parameters increases the control error between the predicted and actual current values. To address these issues, we propose a PID cost function to reduce the impact of motor parameter sensitivity on control performance during weak-magnetic control [30], [31]. The base controller is the traditional FCS-MPC structure shown in Figure 3. The measured stator currents and the rotor position are converted to the d-q reference frame and fed into the prediction model. The inverter switching states are assumed to be admissible, and the d- and q-axis currents are calculated for each admissible switching state and compared with their corresponding reference values using the conventional current-error cost function. The minimum-cost switching state is then selected and fed to the three-phase voltage-source inverter. The switching operation principle of FCS-MPC directly selects the optimal switching state, which serves as the reference condition for evaluating the proposed PID-MPC strategy [32]. The traditional cost function is:

$$O = \left(i_{d(k+2)}^{p} - i_d^*\right)^2 + \left(i_{q(k+2)}^{p} - i_q^*\right)^2 \quad (11)$$

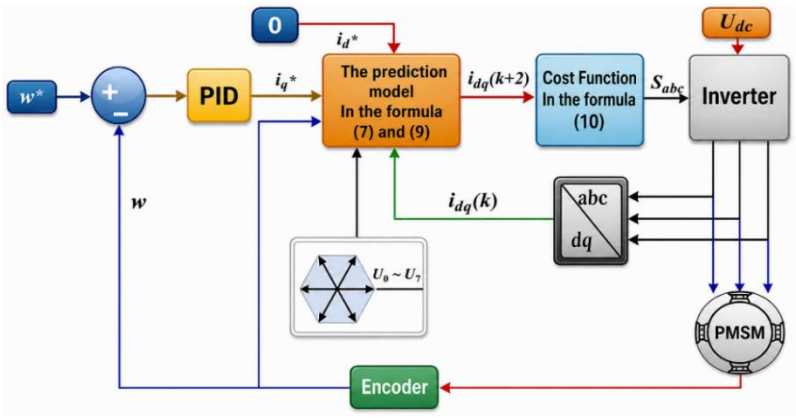

Figure 3. Illustration of the control created on FCS-MPC

3.3. Improved cost function

The idea originates from the PID controller. The control output consists of the sum of three parts: i) Proportional control quickly reflects the error, thus reducing it, but it cannot remove steady-state error; ii) Integral control continuously accumulates its effect, outputting a control quantity to remove steady-state error; and iii) Derivative control predicts the trend of the current error and compensates for the predicted current error [33]. The backward difference equation for the integral term I of the current control error is (12).

$$\begin{cases} I_{d(k)} = I_{d(k-1)} + k_{\mathrm{I}} T_{\mathrm{s}} \left(i^{*}_{d(k)} - i_{d(k)} \right) \\ I_{q(k)} = I_{q(k-1)} + k_{\mathrm{I}} T_{\mathrm{s}} \left(i^{*}_{q(k)} - i_{q(k)} \right) \end{cases} \tag{12}$$

In the formula, $I_{d(k)}$ and $I_{\cdot q(k)}$ the integral terms of the d-axis and q-axis current errors, respectively, and kI is the integral gain factor. Adding this integral term to the traditional cost function theoretically eliminates steady-state error, but in practice it's impossible to eliminate it; it can only reduce it. Ripple error arises from prediction errors in the current change rate due to inaccuracies in the motor model, and the integral term cannot eliminate this prediction error. Furthermore, because the control quantity of FCS-MPC is discontinuous, the derivative term in traditional PID cannot predict it. However, the FCS-MPC cost function includes a deviation term between the predicted output and the reference value. A low-pass filter can soften the reference, avoiding overly aggressive control action and large system overshoot caused by changes to it. Therefore, based on the principle of ripple error, the prediction error caused by the unit change in current in each sampling period is used as the coefficient of the derivative term of the current control error (13).

$$\begin{cases} D'_{d(k)} = \left(k_D \frac{i_{d(k)} - i^{p}_{d(k)}}{i_{d(k)} - i_{d(k-1)}} \right) \\ D'_{q(k)} = \left(k_D \frac{i_{q(k)} - i^{p}_{q(k)}}{i_{q(k)} - i_{q(k-1)}} \right) \end{cases} \tag{13}$$

In (13), k_D is the differential gain coefficient. When a first-order low-pass filter is used, the difference expression is (14):

$$\begin{cases} D'_{d(k)} = (1-\alpha) D'_{d(k-1)} + \alpha \left(k_{\mathrm{D}} \frac{i_{d(k)} - i^{p}_{d(k)}}{i_{d(k)} - i_{d(k-1)}} \right) \\ D'_{q(k)} = (1-\alpha) D'_{q(k-1)} + \alpha \left(k_{\mathrm{D}} \frac{i_{q(k)} - i^{p}_{q(k)}}{i_{q(k)} - i_{q(k-1)}} \right) \end{cases} \tag{14}$$

In the formula, α represents the filter coefficients. Therefore, the differential term D is the product of the coefficients. D' And the predicted change in current. The PID-type coefficients were chosen to optimize transient current tracking, steady-state accuracy, and ripple suppression. The coefficients for the integral, differential, and filtering were fixed at kI = 5.4, kD = 12.05, and α = 0.62, respectively. These values were obtained through iterative simulations in MATLAB/Simulink under the field-weakening condition, accounting for current-tracking accuracy, current distortion, torque ripple, and transient overshoot. The same set of coefficients is applied to all the simulations to ensure a fair comparison between the conventional FCS-MPC and the proposed PID-MPC strategy.

$$\begin{cases} D_{d(k)} = D'_{d(k)} \left(i^{p}_{d(k+2)} - i^{p}_{d(k+1)} \right) \\ D_{q(k)} = D'_{q(k)} \left(i^{p}_{q(k+2)} - i^{p}_{q(k+1)} \right) \end{cases} \tag{15}$$

Therefore, the PID cost function is (16).

$$g = \left(O_{d(k)} + I_{d(k)} + D_{d(k)} \right)^2 + \left(O_{q(k)} + I_{q(k)} + D_{q(k)} \right)^2 \tag{16}$$

In (16), $O_{d(k)}$、$O_{q(k)}$ are the d-axis and q-axis current error terms in the traditional function, respectively.

$$\begin{cases} O_{d(k)} = i^{p}_{d(k+2)} - i^{*}_{d} \\ O_{q(k)} = i^{p}_{q(k+2)} - i^{*}_{q} \end{cases} \tag{17}$$

The suggested PID-MPC control building is displayed in Figure 4. The proposed controller adds extra integral and prediction-based differential error terms to the cost-function estimation as opposed to the traditional FCS-MPC structure. One integral part sums the current tracking error to minimize the persistent steady-state error. In contrast, the other differential part accounts for the predicted current change to eliminate the ripple due to model mismatch. This yields a PID-type cost function, estimated for all possible inverter switching states, and the switching state with the min modified cost is chosen. With this, the proposed structure maintains the direct finite-control-set operation of conventional FCS-MPC while enhancing system robustness under parameter mismatches.

Figure 5 shows the MATLAB/Simulink model of an MPC-based PMSM drive control system. It includes a speed reference, error calculation, and feedback from the motor speed. The MPC controller receives the reference currents, measured currents, rotor position, rotor speed, and DC-link voltage. The controller generates optimized switching signals to send to the PWM and three-phase inverter. The inverter drives the PMSM, and Clarke-Park transformations convert the motor currents. The overall model includes speed control, predictive current control, PWM, inverter switching, and PMSM feedback in a closed loop.

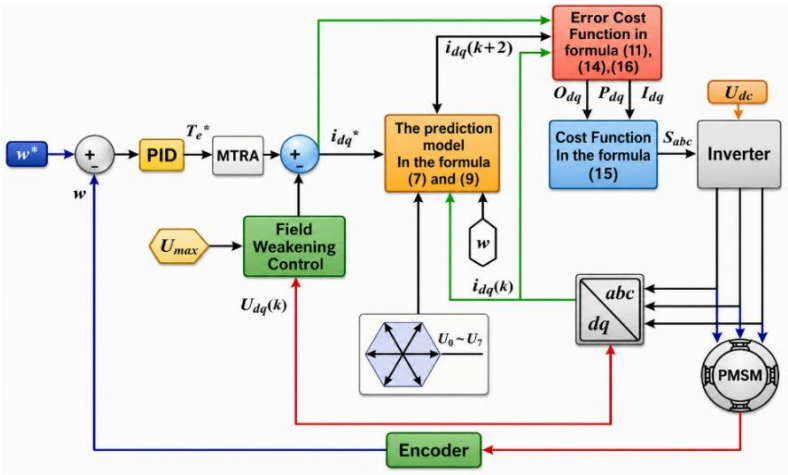

Figure 4. Control created on PID-MPC

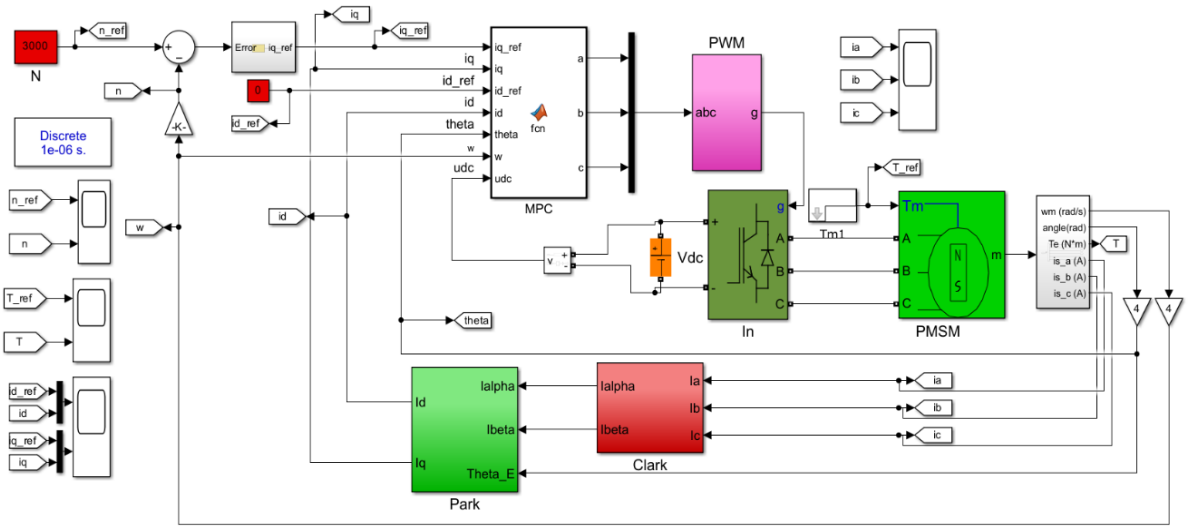

Figure 5. MATLAB/Simulink model of an MPC-based PMSM

4. RESULTS AND DISCUSSION

Several MATLAB/Simulink simulations were performed to fully assess the efficiency and stability of the proposed (PID-MPC) approach when used for field-weakening operation. A systematic comparison of the proposed PID-MPC controller with the conventional (FCS-MPC) strategy, based on the conventional cost function, focused on current-tracking accuracy, dynamic response, and robustness during high-speed field-weakening operation. The system parameters were kept the same across both control strategies to ensure a comparable and consistent comparison. The simulation model parameters were set as follows: four pole pairs, 6.552 mH d-axis inductance, 6.552 mH q-axis inductance, 0.901 Ω stator resistance, and 0.11 Wb permanent-magnet flux linkage. The reference speed is 3000 rpm, the applied load torque is 2.4 Nm, and the DC-link voltage is fixed at 311 V. These values reflect representative operating conditions for testing drive behavior under field weakening and provide a valid comparison between the standard FCS-MPC and the proposed

PID-MPC approaches. Under these conditions, the suggested PID-MPC approach is quantitatively and qualitatively compared with the standard control approach using simulation results for current-tracking error, speed regulation, electromagnetic torque response, transient characteristics, and overall control robustness. For the same assessment, both the controller and the PMSM model were evaluated with the same PMSM model, inverter configuration, DC-link voltage, orientation speed, load torque, sampling conditions, and operating conditions.

The standard FCS-MPC is chosen as the reference model because the proposed contribution does not alter the FCS-MPC structure but modifies the objective function. This comparison therefore considers only the effect of the proposed cost-function formulation (i.e., the change from a quadratic to a PID formulation), not changes to the predictive-control architecture. The performance assessment includes current waveform quality, THD, torque overshoot, torque ripple, and overall dynamic behavior.

Figures 6 and 7 show the three-phase stator current waveforms generated by the conventional FCS-MPC and PID-MPC algorithms, respectively. In this analysis, the PMSM operates at its rated speed of 3000 rpm under its specified rated load conditions. A thorough comparison between the outputs of the two algorithms reveals that the application of the PID-MPC algorithm results in a significant reduction of current ripple, an enhancement in the sinusoidal quality of the waveform, and a noticeable decrease in the current distortion rate, thereby indicating a superior performance of the PID-MPC approach over the traditional method. These findings underscore the usefulness of the PID-MPC procedure in optimizing PMSM operational characteristics, particularly were maintaining waveform integrity and minimizing distortion are paramount to improving overall system efficiency and reliability.

The suggested PID-MPC strategy improves the current waveform quality, as shown in the quantitative results in Figures 8 and 9. The standard FCS-MPC generates a 3-phase current THD of 13.09%, while the suggested PID-MPC generates a 3-phase current THD of 4.79%. This represents about a 63.4% reduction in THD. The improvement is due to the inclusion of the extra integral and prediction-based differential terms in the cost function. The integral component eliminates persistent current-tracking deviations, and the differential component responds to system-predicted current variations and helps suppress high-frequency current ripple. Thus, the suggested cost-function formulation improves the quality of the current while preserving the MPC structure.

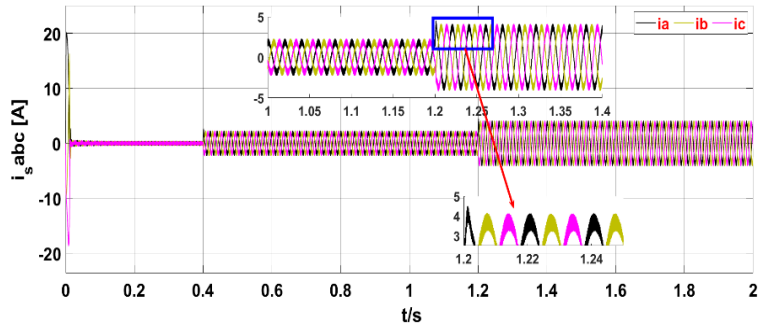

Figure 6. Three-phase current waveforms with FCS-MPC

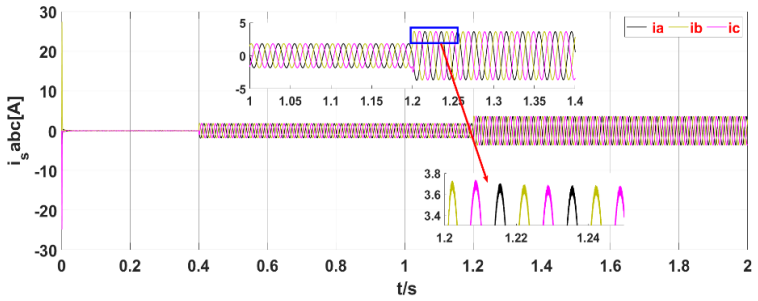

Figure 7. Three-phase current waveforms with PID-MPC

The torque reactions from the standard FCS-MPC and suggested PID-MPC are displayed in Figures 10 and 11, respectively. It is noted that the conventional FCS-MPC exhibits significant torque

oscillations in both the transient and steady-state operating ranges. The PID-MPC offers a significantly more stable torque response. From the numerical comparison shown in Figure 12, the torque overshoot decreases from 1.500 Nm to 1.234 Nm, approximately 17.7% less. Most importantly, the torque ripple reduces by 88.5% when switching from conventional FCS-MPC to PID-MPC, from 50.00% to 5.75%. The results show that the proposed cost function effectively suppresses oscillatory behavior and regulates torque under the considered field-weakening condition.

The performance of the standard FCS-MPC and the suggested PID-MPC in terms of torque is illustrated in Figure 12. This method minimizes the torque overshoot from 1.500 Nm to 1.234 Nm and substantially reduces the torque ripple from 50.00% to 5.75%, demonstrating a remarkable improvement in quality and dynamic performance. The FCS-MPC methodology, based on a foundational analysis of the PID-MPC control principle, systematically evaluates these two control paradigms in terms of THD, harmonic content, current overshoot, and torque ripple, as shown in Table 2. The PID-MPC framework notably reduces response latency, thereby improving the system's robustness against interference. The PID-MPC shows clear advantages in reducing ripple associated with current harmonic distortion.

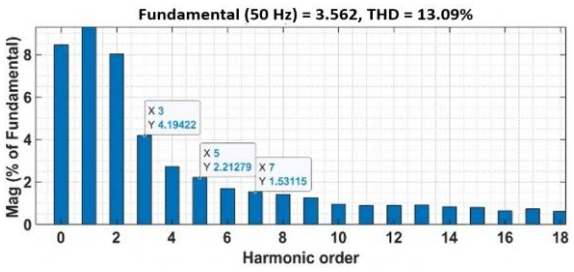

Figure 8. THD with FCS-MPC

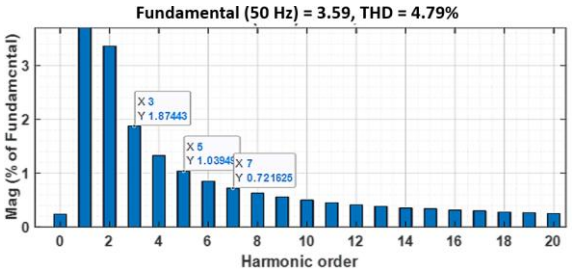

Figure 9. THD with PID-MPC

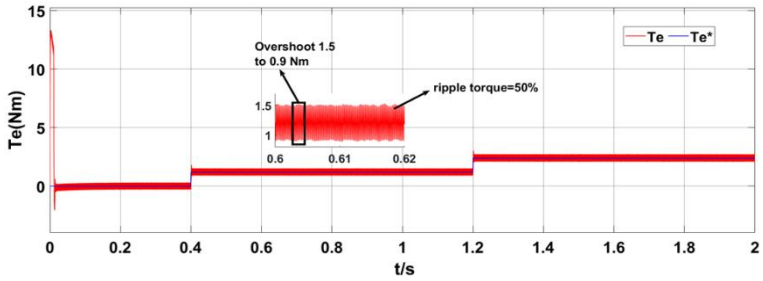

Figure 10. Torque response curve with FCS-MPC

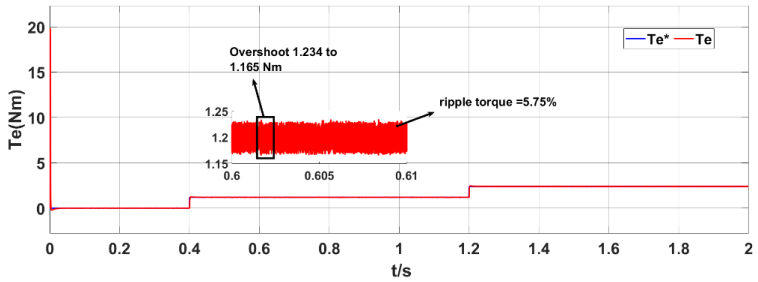

Figure 11. Torque response curve with PID-MPC

Table 2. Comparison between the two algorithms

Results	FCS-MPC	PID-MPC
THD	13.09%	4.79%
Overshoot of torque	1.5 to 0.9 Nm	1.234 to 1.165Nm
Ripple of torque	50%	5.75%
harmonic	High	Low

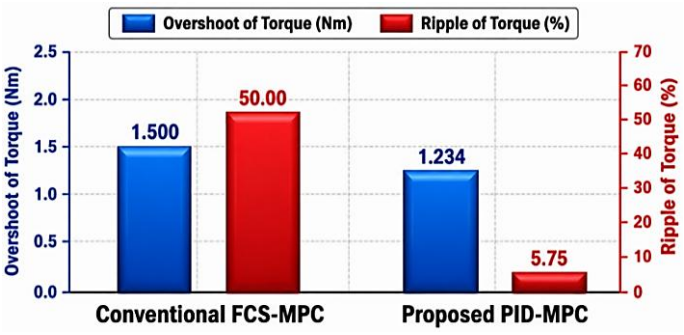

Figure 12. Compares the torque performance

5. CONCLUSION

This paper applies PID-MPC to field-weakening control of a PMSM (motor speed control system) to address the parameter-sensitivity problem of the FCS-MPC strategy based on the traditional objective function. Based on the conventional objective function, the PID-based cost function reduces steady-state current control error by increasing the integral error cost. It suppresses ripple current error by increasing the differential error cost, thus improving the system's parameter robustness. Simulation results show that the PID-MPC-based PMSM speed control system exhibits good dynamic performance and superior robustness to parameter variations compared to the standard cost-function FCS-MPC, making it suitable for operation over a wide speed range in electric vehicles. Although the simulation results were encouraging, this work did not include experimental or HIL validation. Further studies will thus be carried out on a real-time control platform, and the performance of the proposed PID-MPC approach will be analyzed experimentally for parameter variations, inverter nonidealities, measurement noise, computational delays, and wide-speed field-weakening operation. This validation will further support the feasibility and stability of the proposed method.

ACKNOWLEDGMENTS

The authors thank everyone who provided technical and academic assistance in preparing this work.

FUNDING INFORMATION

This study is funded by itself, according to the investigators.

AUTHOR CONTRIBUTIONS STATEMENT

This journal uses the Contributor Roles Taxonomy (CRediT) to recognize individual author contributions, reduce authorship disputes, and facilitate collaboration.

Name of Author	C	M	So	Va	Fo	I	R	D	O	E	Vi	Su	P	Fu
Yasameen H. Abdulrida	✓			✓	✓	✓		✓		✓			✓	
Islam Khalid		✓		✓		✓		✓	✓		✓	✓		
Othman J. Alhayali	✓		✓				✓			✓			✓	✓

C : **C**onceptualization
M : **M**ethodology
So : **So**ftware
Va : **Va**lidation
Fo : **Fo**rmal analysis
I : **I**nvestigation
R : **R**esources
D : **D**ata Curation
O : Writing - **O**riginal Draft
E : Writing - Review & **E**diting
Vi : **Vi**sualization
Su : **Su**pervision
P : **P**roject administration
Fu : **Fu**nding acquisition

CONFLICT OF INTEREST STATEMENT

The authors state no conflict of interest.

DATA AVAILABILITY

Data availability is not applicable to this paper as no new data were created or analyzed in this study.

REFERENCES

[1] M. R. Nikzad, B. Asaei, and S. O. Ahmadi, "Discrete duty-cycle-control method for direct torque control of induction motor drives with model predictive solution," *IEEE Transactions on Power Electronics*, vol. 33, no. 3, pp. 2317–2329, Mar. 2018, doi: 10.1109/TPEL.2017.2690304.

[2] S. T. Bahar and H. Qiu, "Amelioration of traditional pi boost converter utilizing linear active disturbance rejection controller-mode predictive control strategy," *International Journal of Robotics and Control Systems*, vol. 6, no. 1, pp. 305–323, Jan. 2026, doi: 10.31763/ijrcs.v6i1.2364.

[3] S. S. Yeoh, T. Yang, L. Tarisciotti, C. I. Hill, S. Bozhko, and P. Zanchetta, "Permanent-magnet machine-based starter-generator system with modulated model predictive control," *IEEE Transactions on Transportation Electrification*, vol. 3, no. 4, pp. 878–890, Dec. 2017, doi: 10.1109/TTE.2017.2731626.

[4] Z. Zhou, C. Xia, Y. Yan, Z. Wang, and T. Shi, "Torque ripple minimization of predictive torque control for PMSM with extended control set," *IEEE Transactions on Industrial Electronics*, vol. 64, no. 9, pp. 6930–6939, Sep. 2017, doi: 10.1109/TIE.2017.2686320.

[5] V. M. Bida, D. V. Samokhvalov, and F. S. Al-Mahturi, "PMSM vector control techniques - a survey," in *Proceedings of the 2018 IEEE Conference of Russian Young Researchers in Electrical and Electronic Engineering, ElConRus 2018*, Jan. 2018, pp. 577–581, doi: 10.1109/EIConRus.2018.8317164.

[6] S. T. Bahar, W. Wang, and H. Qiu, "AI-enhanced model predictive and active disturbance rejection control for high-performance permanent magnet synchronous motor drives," *Energies*, vol. 19, no. 11, May 2026, doi: 10.3390/en19112574.

[7] W. Xu, A. K. Junejo, Y. Liu, M. G. Hussien, and J. Zhu, "An efficient anti-disturbance sliding-mode speed control method for PMSM drive systems," *IEEE Transactions on Power Electronics*, vol. 36, no. 6, pp. 6879–6891, Jun. 2021, doi: 10.1109/tpel.2020.3039474.

[8] T. Il Yeam and D. C. Lee, "Design of sliding-mode speed controller with active damping control for single-inverter dual-PMSM drive systems," *IEEE Transactions on Power Electronics*, vol. 36, no. 5, pp. 5794–5801, May 2021, doi: 10.1109/TPEL.2020.3028601.

[9] S. T. Bahar and R. G. Omar, "Permanent magnet synchronous motor torque ripple reduction using predictive torque control," *Journal of Engineering and Sustainable Development*, vol. 27, no. 3, pp. 394–406, 2023, doi: 10.31272/jeasd.27.3.9.

[10] L. He, F. Wang, and D. Ke, "FPGA-based sliding-mode predictive control for PMSM speed regulation system using an adaptive ultra local model," *IEEE Transactions on Power Electronics*, vol. 36, no. 5, pp. 5784–5793, May 2021, doi: 10.1109/TPEL.2020.3028545.

[11] J. Shen, X. Wang, Z. Zhang, S. Ren, D. Ma, and D. Xiao, "Research on the application of dual three-phase PMSM in renewable energy system," in *2023 26th International Conference on Electrical Machines and Systems, ICEMS 2023*, Zhuhai, China, 2023, pp. 3475–3479, doi: 10.1109/ICEMS59686.2023.10344728.

[12] M. K. Ismael, S. T. Bahar, and A. A. Abdullah, "Harmonic elimination method for permanent magnet synchronous motor utilizing active disturbance rejection control," *Proceedings of Engineering and Technology Innovation*, vol. 30, pp. 11–23, Jun. 2025, doi: 10.46604/peti.2024.14386.

[13] W. Tong, L. Sun, S. Wu, M. Hou, and R. Tang, "Analytical model and experimental verification of permanent magnet eddy current loss in permanent magnet machines with nonconcentric magnetic poles," *IEEE Transactions on Industrial Electronics*, vol. 69, no. 9, pp. 8815–8824, Sep. 2022, doi: 10.1109/TIE.2021.3111573.

[14] H. Zhao, C. Liu, Z. Song, and W. Wang, "Exact modeling and multiobjective optimization of vernier machines," *IEEE Transactions on Industrial Electronics*, vol. 68, no. 12, pp. 11740–11751, Dec. 2021, doi: 10.1109/TIE.2020.3044785.

[15] M. Chen, F. Wang, L. He, D. Ke, K. Zuo, and J. Rodriguez, "Predictive current control of permanent magnet synchronous motor based on an adaptive internal model observer," in *2020 IEEE 9th International Power Electronics and Motion Control Conference, IPEMC 2020 ECCE Asia*, Nanjing, China, 2020, pp. 2567–2571, doi: 10.1109/IPEMC-ECCEAsia48364.2020.9368203.

[16] I. Khalid, O. J. Alhayali, and S. Aljanabi, "Adaptive sliding-mode observer-assisted model predictive direct speed control for PMSM drives under parameter uncertainty and load disturbances," *Buletin Ilmiah Sarjana Teknik Elektro*, vol. 8, no. 4, pp. 1057–1075, Aug. 2026, doi: 10.12928/biste.v8i4.16737.

[17] S. T. Bahar and R. G. Omar, "Torque ripple alleviation of a five-phase permanent magnet synchronous motor using predictive torque control method," *International Journal of Power Electronics and Drive Systems*, vol. 13, no. 4, pp. 2207–2215, Dec. 2022, doi: 10.11591/ijpeds.v13.i4.pp2207-2215.

[18] S. A. Davari, F. Wang, and R. M. Kennel, "Robust deadbeat control of an induction motor by stable MRAS speed and stator estimation," *IEEE Transactions on Industrial Informatics*, vol. 14, no. 1, pp. 200–209, Jan. 2018, doi: 10.1109/TII.2017.2756900.

[19] Z. Mynar, L. Vesely, and P. Vaclavek, "PMSM model predictive control with field-weakening implementation," *IEEE Transactions on Industrial Electronics*, vol. 63, no. 8, pp. 5156–5166, Aug. 2016, doi: 10.1109/TIE.2016.2558165.

[20] Y. Zhang, B. Zhang, H. Yang, M. Norambuena, and J. Rodriguez, "Generalized sequential model predictive control of IM drives with field-weakening ability," *IEEE Transactions on Power Electronics*, vol. 34, no. 9, pp. 8944–8955, Sep. 2019, doi: 10.1109/TPEL.2018.2886206.

[21] S. T. Bahar and R. A. Abd-Alhmeed, "Reduce-complexity of predictive current control for a 3-phase voltage source inverter," *Journal of Techniques*, vol. 7, no. 3, pp. 16–25, Sep. 2025, doi: 10.51173/jt.v7i3.2621.

[22] H. Yang, Y. Zhang, and W. Shen, "Predictive current control and field-weakening operation of SPMSM drives without motor parameters and dc voltage," *IEEE Journal of Emerging and Selected Topics in Power Electronics*, vol. 10, no. 5, pp. 5635–5646, Oct. 2022, doi: 10.1109/JESTPE.2022.3167273.

[23] M. S. Rafaq and J.-W. Jung, "A comprehensive review of state-of-the-art parameter estimation techniques for permanent magnet synchronous motors in wide speed range," *IEEE Transactions on Industrial Informatics*, vol. 16, no. 7, pp. 4747–4758, Jul. 2020, doi: 10.1109/TII.2019.2944413.

[24] P. Karamanakos and T. Geyer, "Guidelines for the design of finite control set model predictive controllers," *IEEE Transactions on Power Electronics*, vol. 35, no. 7, pp. 7434–7450, Jul. 2020, doi: 10.1109/TPEL.2019.2954357.

[25] Q. Dong, B. Wang, L. Xia, Y. Yu, M. Tian, and D. Xu, "A virtual voltage field-weakening scheme of trajectory correction for PMSM model predictive control," *IEEE Transactions on Power Electronics*, vol. 38, no. 3, pp. 3044–3056, Mar. 2023, doi: 10.1109/TPEL.2022.3219811.

[26] X. Fang, S. Lin, X. Wang, Z. Yang, F. Lin, and Z. Tian, "Model predictive current control of traction permanent magnet synchronous motors in six-step operation for railway application," *IEEE Transactions on Industrial Electronics*, vol. 69, no. 9, pp. 8751–8759, Sep. 2022, doi: 10.1109/TIE.2021.3114695.

[27] J. Holtz, "Predictive finite-state control - when to use and when not," *IEEE Transactions on Power Electronics*, vol. 37, no. 4, pp. 4225–4232, Apr. 2022, doi: 10.1109/TPEL.2021.3121277.

[28] S. Zhao, X. Huang, Y. Fang, and H. Zhang, "DC-link-fluctuation-resistant predictive torque control for railway traction permanent magnet synchronous motor in the six-step operation," *IEEE Transactions on Power Electronics*, vol. 35, no. 10, pp. 10982–10993, Oct. 2020, doi: 10.1109/TPEL.2020.2975497.
[29] S. T. Bahar, B. Zhang, W. Wang, and H. Qiu, "Dimensionless multi-objective model predictive current control with harmonic subspace suppression for six-phase PMSM drives," *World Electric Vehicle Journal*, vol. 17, no. 9, Sep. 2026, doi: 10.3390/wevj17090461.
[30] J. Chen, J. Li, and R. Qu, "Maximum-torque-per-ampere and magnetization-state control of a variable-flux permanent magnet machine," *IEEE Transactions on Industrial Electronics*, vol. 65, no. 2, pp. 1158–1169, Feb. 2017, doi: 10.1109/TIE.2017.2733494.
[31] Z. Yin, L. Li, F. Gao, J. Liu, and Y. Zhang, "Robust current predicted control of permanent magnet synchronous motors based on novel sliding model observer," in *Proceedings of 2021 IEEE 4th International Electrical and Energy Conference, CIEEC 2021*, Wuhan, China, 2021, pp. 1–6, doi: 10.1109/CIEEC50170.2021.9510238.
[32] S. T. Bahar and D. R. Neama, "Improved direct torque control utilizing model predictive control approach for permanent magnet synchronous motor," *Al-Iraqia Journal for Scientific Engineering Research*, vol. 3, no. 2, pp. 57–64, Jul. 2024, doi: 10.58564/IJSER.3.2.2024.179.
[33] M. Gu, Z. Wang, and B. Wang, "Optimization of torque ripple for low-carrier-ratio dual three-phase PMSM with pulse pattern control," *IEEE Transactions on Power Electronics*, vol. 38, no. 12, pp. 15091–15096, Dec. 2023, doi: 10.1109/TPEL.2023.3298961.

BIOGRAPHIES OF AUTHORS



Yasameen H. Abdulrida received her Bachelor of Science and Master of Science degrees from the Department of Electromechanical Engineering at the University of Technology, Baghdad, Iraq, in 2012 and 2023, respectively. She is currently a faculty member at Ibn Sina University of Medical and Pharmaceutical Sciences, Baghdad, Iraq. Her research interests include power engineering, electrical machines, systems and control theory, composite materials, and the electrical and mechanical properties of materials. She can be contacted at email: yasameen.aarajy@ibnsina.edu.iq.



Islam Khalid received her Bachelor of Science degree from the College of Engineering at the University of Diyala, Diyala, Iraq, in 2011, and her Master of Science degree from the College of Engineering at Cairo University, Cairo, Egypt, in 2021. She is currently a faculty member in the Department of Power and Electrical Machines at the University of Diyala, Iraq. Her research interests include power electronics, systems and control theory, electrical machines and drives, and electrical power systems. She can be contacted at email: islam.kh@uidiyala.edu.iq.



Othman J. Alhayali is a faculty member at the Renewable Energy Research Center, University of Anbar, Iraq. His research focuses on electrical power engineering, renewable energy systems, and electrical machines, with particular emphasis on photovoltaic (PV) systems and solar energy applications. His research interests also include system optimization, inverter control, and performance evaluation of solar and hybrid power systems. He can be contacted at email: othman.jaseem@uoanbar.edu.iq.